Synthesis and Characterization of Silica, Silver-Silica, and Zinc Oxide-Silica Nanoparticles for Evaluation of Blood Biochemistry, Oxidative Stress, and Hepatotoxicity in Albino Rats

Arooj Ali, Saba Saeed,* Riaz Hussain, Gulnaz Afzal, Abu Baker Siddique, Gulnaz Parveen, Murtaza Hasan,* and Giovanni Caprioli*
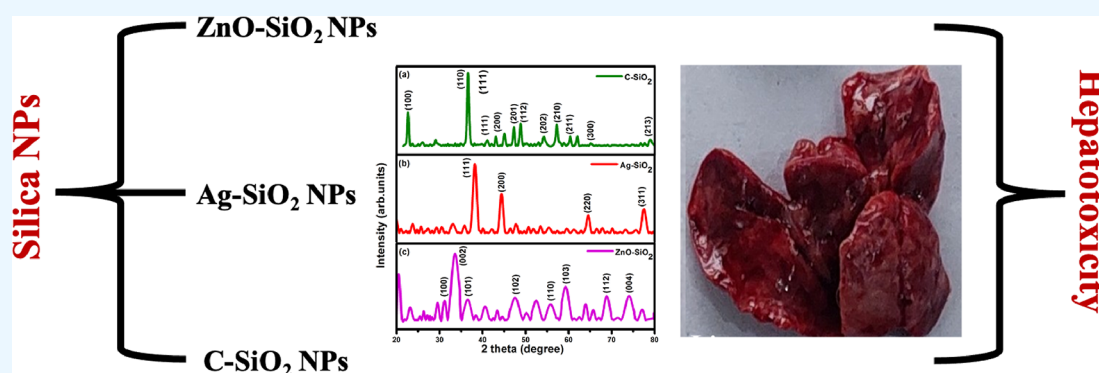
Read Online

ACCESS | Metrics & More | Article Recommendations | Supporting Information

ABSTRACT: Evaluation of nanoparticles (NPs) for biomedical applications has received a lot of attention for detailed study on pharmacokinetics prior to clinical application. In this study, pure C-SiO$_2$ (crystalline silica) NPs and SiO$_2$ nanocomposites with silver (Ag) and zinc oxide (ZnO) were prepared by utilizing different synthesis routes such as sol−gel and co-precipitation techniques. The prepared NPs showed highly crystalline nature as confirmed by X-ray diffraction analysis where average crystallite sizes of 35, 16, and 57 nm for C-SiO$_2$, Ag-SiO$_2$, and ZnO-SiO$_2$ NPs, respectively, were calculated. Fourier transform infrared analysis confirmed the presence of functional groups related to the chemicals and procedures used for sample preparation. Due to agglomeration of the prepared NPs, the scanning electron microscope images showed large particle sizes when compared to their crystalline sizes. The optical properties of the prepared NPs such as absorption were obtained with UV−Vis spectroscopy. For in vivo biological evaluation, albino rats, both male and female, kept in different groups were exposed to NPs with 500 μg/kg dose. Hematological, serum biochemistry, histo-architecture, oxidative stress biomarkers, and antioxidant parameters in liver tissues along with various biomarkers for the evaluation of erythrocytes were estimated. The results on hemato-biochemistry, histopathological ailments, and oxidative stress parameters exhibited 95% alteration in the liver and erythrocytes of C-SiO$_2$ NPs-treated rats while 75 and 60% alteration in the liver tissues of rats due to exposure to Ag-SiO$_2$ and ZnO-SiO$_2$ NPs, respectively, when compared with the albino rats of the control (untreated) group. Therefore, the current study showed that the prepared NPs had adverse effects on the liver and erythrocytes causing hepatotoxicity in the albino rats in respective order C-SiO$_2$ > Ag SiO$_2$ > ZnO-SiO$_2$. As the C-SiO$_2$ NPs appeared to be the most toxic, it has been concluded that coating SiO$_2$ on Ag and ZnO reduced their toxicological impact on albino rats. Consequently, it is suggested that Ag-SiO$_2$ and ZnO-SiO$_2$ NPs are more biocompatible than C-SiO$_2$ NPs.

1. INTRODUCTION

Nanotechnology is a rapidly developing field with a diverse range of applications in medicine, pesticides, cosmetics, biomedical sectors, bioengineering, and optoelectronic industries.[1−3] Inspite of advancements in nanomaterials, the rate of nanoparticle (NPs) exposure is increasing and they can enter the living organism *via* ingestion, inhalation, infusion, and dermal penetration.[4,5] From the biomedical point of view, toxicological evaluation of the NPs reveals their distinctive physiochemical characteristics. The appraisal of the damaging effects of NPs requires many configurations for both in vitro and in vivo

studies.[6,7] There are numerous reports on the in vitro toxicity evaluation of NPs,[8,9] but nanotoxicity-based in vivo studies are of vital importance. There are several different mechanisms by
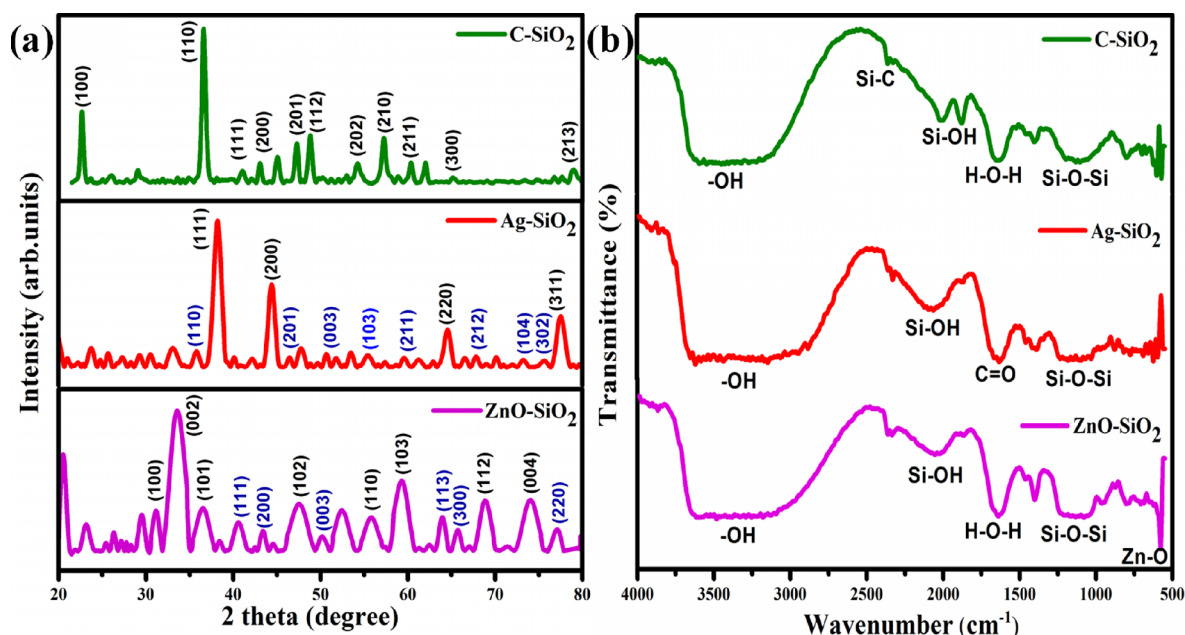
Figure 1. (a) XRD spectra of C-SiO$_2$ NPs (green), Ag-SiO$_2$ NPs (red), and ZnO-SiO$_2$ NPs (magenta). (b) FTIR spectra of C-SiO$_2$ NPs (green), Ag-SiO$_2$ NPs (red), and ZnO-SiO$_2$ NPs (magenta).

which the nanomaterials induce toxicity in animals. However, induction of oxidative stress due to the formation of free radicals is the key process by which various natural and synthetic materials induce deleterious effects in tissues. Among different NPs, SiO$_2$ NPs are widely used in biomedical applications including labeling, biosensors, medical diagnosis, in vivo imaging, degradation of toxicants, and delivery of drugs and antibodies.[10−12] Apart from the reported toxicity of C-SiO$_2$, its coating and mixing are frequently done to enhance the stabilization of NPs. This is usually done for chemical inertness enhancement, avoidance of agglomeration, temperature resistance, high biocompatibility, and resistance to decomposition.[13] SiO$_2$ surfaces can also be easily functionalized with carboxyl (R-COOH), thiol (−SH), and amine (R-NH$_2$ R-NH$_2$) groups for biomedical applications.[14] Furthermore, coating SiO$_2$ NPs with Ag, yttrium oxide (Y$_2$O$_3$), and ZnO[15] showed improved biocompatibility. Based on biomedical studies, it has been reported that the Ag NPs while traveling along the blood stream accumulate in different body tissues and organs, making these organs susceptible to damage and altering the physiological functions.[16,17] However, when compared to other NPs, Ag NPs are more accessible due to their room temperature stability as well as their affordable precursors.[18] Despite the toxic impacts, aqueous solution of Ag NPs deposited in different media such as SiO$_2$ or composites has been used as an effective sterilizing tool in agriculture and veterinary practices.[19,20] The effectiveness and efficiency of the NPs are increased in a specific treated atmosphere through a variety of methods of modification.[21−23] It has been reported that Ag and SiO$_2$ NPs behave differently in biological systems, while studies have also indicated that SiO$_2$-coated Ag NPs are less toxic than individual Ag NPs,[24] but Ag-SiO$_2$ NPs have not been investigated in detail when compared to SiO$_2$ or Ag NPs separately. Meanwhile, ZnO NPs have distinct properties including increased reactivity and upgraded UV filtering ability that distinguish them from bulk ZnO.[2,25,26] In spite of the numerous benefits of ZnO NPs, their utilization has few restrictions, such as ZnO NPs discharging Zn^{2+} ions, which are responsible for the cytotoxic effects.[27] Therefore, an active

area of research is the development of techniques to reduce the toxicity of ZnO NPs without modifying their core properties.[28,29] Similar to SiO$_2$-coated Ag NPs, the stability and dispersibility of SiO$_2$-coated ZnO NPs were increased, thereby broadening the range of their applications. The coating of ZnO NPs with amorphous SiO$_2$ reduced the dissolution of Zn^{2+} ions in biological medium as well as reduced the cell cytotoxicity and DNA damage. The biocompatibility, stability, surface area, morphology, and size are the distinctive properties of Au, Zn, Cu, Ni, and SiO$_2$ NPs.[30] Nanomaterials have demonstrated significant promise in a wide range of fields, from technology to biological sciences and from cellular to molecular and genetic processes.[31−33] However, there is a significant gap in knowledge concerning the precise mechanism of NPs-induced oxidative stress, and little information about toxic effects of Ag-SiO$_2$ is available in the literature. A comparative study related to the toxic effects of C-SiO$_2$, Ag-SiO$_2$, and ZnO-SiO$_2$ has not been reported. Subsequently, for the first time, adverse effects of these prepared NPs on blood biomarkers, serum chemistry, histopathology, and oxidative and antioxidant enzymes in the liver and blood of albino rats have been observed in this current study.

2. RESULTS AND DISCUSSION

Engineered NPs are commonly and persistently utilized as coating materials in cosmetics, pesticides, and different drugs. This implies that people are increasingly exposed to different types of fabricated NPs in daily life. Although nanomaterials have numerous scientific applications, their widespread use poses potential risks to the atmosphere and living organisms, which limits their use in biomedicine.[34] NPs have toxic effects on tissues, metabolic process of cells, and subcellular and multiple organs in living organisms because of their small size and ability to cross physical obstacles.[35] Therefore, the purpose of this study is to investigate the effects of NPs on hematology, serum biochemistry, histopathology, oxidative stress, and antioxidant enzymes in the liver and different biomarkers of erythrocytes of NPs-treated rats.
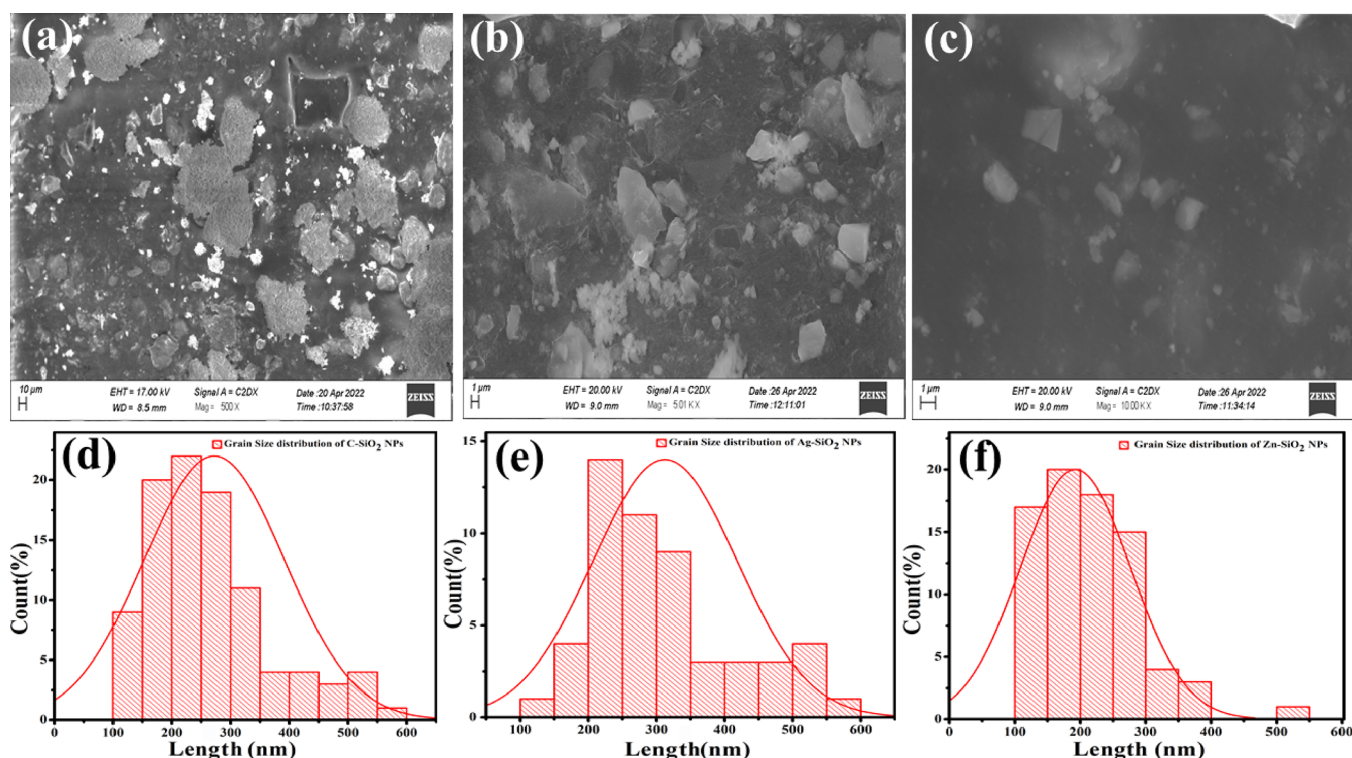
Figure 2. SEM images showing the morphology of (a) C-SiO$_2$ NPs, (b) Ag-SiO$_2$ NPs, and (c) ZnO-SiO$_2$ NPs. Grain size distribution of (d) C-SiO$_2$ NPs, (e) Ag-SiO$_2$ NPs, and (f) ZnO-SiO$_2$ NPs.

2.1. Structural Analysis of Silica, Silver-Silica, and Zinc-Silica Nanoparticles.

For C-SiO$_2$, the XRD showed peaks at 21.8, 36, 40.3, 42.6, 46.7, 48.7, 53.9, 56.9, 61, 65.2, and 79° associated with the (100), (110), (111), (200), (201), (112), (202), (210), (211), (300), and (213) planes, respectively, shown with green color in Figure 1a. All these peaks belong to C-SiO$_2$ as confirmed from the JCPD card: 00-046-1045. The Scherrer formula was utilized to calculate the crystalline size of the NPs[36]

$$D = \frac{K\lambda}{\beta \cos \theta} \tag{1}$$

where D is the crystalline size of particles, K is a constant, λ is the wavelength of X-ray Cu (kα) radiation (0.154056 nm), β is the full width at half-maximum, and θ is the Bragg's angle. The calculated average crystallite size of C-SiO$_2$ NPs was 35 nm. The XRD pattern of the prepared C-SiO$_2$ NPs possessed a hexagonal structure. For Ag-SiO$_2$ NPs, the XRD pattern prominently shows the diffraction peaks related to the FCC structure of Ag (JCPDS card no. 04-0783) in Figure 1a (red color). The peaks at 38.3, 44.5, 64.7, and 77.5° are related to the (111), (200), (220), and (311) crystalline phases of Ag. The remaining XRD peaks at 35.7, 46.5, 50.7, 55.4, 59.5, 67.8, 73.3, and 75.5° are associated with the (110), (201), (003), (103), (211), (212), (104), and (302) planes, respectively, and are due to the presence of C-SiO$_2$ in the sample. Hence, we safely confirm the crystalline nature of the Ag-SiO$_2$ NPs sample.[37] The calculated average crystallite size for Ag-SiO$_2$ NPs was 16 nm. The XRD pattern of Ag-SiO$_2$ NPs revealed a change in SiO$_2$ morphology after the reaction of SiO$_2$ with silver acetate.[37,38] The XRD pattern of ZnO-SiO$_2$ NPs showed diffraction peaks related to the hexagonal wurtzite ZnO (JCPDS card no. 36-1451). The diffraction peaks at 31.1, 33.5, 36.7, 47.9, 55.8, 59.5, 68.9, and 74.4° are related to the (100),

(002), (101), (102), (110), (103), (112), and (004) crystalline phases of ZnO, respectively, as shown in Figure 1a (magenta color). The remaining peaks at 40.6, 43.4, 50.3, 64.0, 65.7, and 77.1° associated with (111), (200), (003), (113), (300), and (220), respectively, are attributed to the C-SiO$_2$ in the sample. Here again, we confirm the crystalline nature of the ZnO-SiO$_2$ NPs sample. This study is also consistent with Abdel Messih et al. who also prepared ZnO-SiO$_2$ NPs.[39] An average crystallite size of 57 nm was calculated for these NPs. The XRD patterns of the earlier study indicated the change in the structure of SiO$_2$ after reaction with zinc acetate.[40] Almost all the major peaks in the XRD spectrum of ZnO-SiO$_2$ NPs are attributed to the hexagonal ZnO and SiO$_2$ nanocomposite.

The FTIR spectrum of C-SiO$_2$ NPs shown with green color in Figure 1b confirmed the presence of functional groups that are associated with the formation of C-SiO$_2$. A broad peak ranging from 3165 to 3633 cm^{-1} and a peak at 1680 cm^{-1} are from the −OH bonding and stretching vibrations. The band at 2361 cm^{-1} is the Si−C bonding. The band around 1870 cm^{-1} is associated with the Si-OH vibrations. Furthermore, the bands at 1100 and 791 cm^{-1} are assigned to the asymmetric and symmetric Si-O-Si stretching vibration. The FTIR spectrum of C-SiO$_2$ NPs is comparable with the previous FTIR studies of nano-SiO$_2$.[41] Figure 1b (red color) shows the FTIR spectrum for the Ag-SiO$_2$ NPs. The pattern confirms the presence of functional groups associated with these NPs. The broad band ranging from 2906 to 3650 cm^{-1} is due to −OH vibration mode. The band around 2071 cm^{-1} is because of the Si-OH stretching bond. The COO- group is responsible for the peak at 1630 cm^{-1}, which is caused by reaction of TEOS with silver acetate. The peak at 1106 cm^{-1} is due to the Si-O-Si stretching vibration. The peaks are attributed to the effective condensation of SiO$_2$, resulting in the production of the Ag-SiO$_2$ nanocomposite and supported by a previous study.[38]

Figure 1b (magenta color) shows the FTIR spectrum for the ZnO-SiO$_2$ NPs. The pattern confirms the presence of functional groups associated with these NPs. The broad band ranging from 3063 to 3605 cm^{-1} and a peak around 1637 cm^{-1} are due to the −OH vibration mode. The band around 2045 cm^{-1} is from the Si-OH stretching bond. The peak at 1133 cm^{-1} is due to the Si-O-Si stretching vibration bonding, and the band at 570 cm^{-1} is attributed to the presence of Zn−O bonding. The functional group in the FTIR spectrum of ZnO-SiO$_2$ confirms the existence of the ZnO-SiO$_2$ nanocomposite, and the results are in agreement with Praseptiangga et al.[42]

2.2. Morphology of Silica and Silica-Based Nanoparticles. SEM was utilized to determine the grain size of the particles and the morphology of the prepared samples.

Figure 2a shows the SEM image of C-SiO$_2$ NPs. C-SiO$_2$ NPs that experienced calcination at a temperature of 1100 °C for 1 h displayed particle growth, larger grains with a denser structure, and fewer grain boundaries. Formation of large particles was the reason behind the disappearance of grain boundaries. The biggest agglomerate that appeared in the SEM image shows some hollow spots, which supports that on further magnification, the structure may appear porous as reported by Hussain et al.[43] The histogram plot is shown in Figure 2d, and the average grain/particle size was calculated and found to be 272 ± 119 nm. The obtained results resemble the earlier studies on differently prepared SiO$_2$ NPs.[44,45]

The shape and particle size distribution of Ag-SiO$_2$ NPs were also revealed through the SEM images presented in Figure 2b. The shape of these NPs appeared to be irregular including rectangular, oval, and elongated. The average particle size of Ag-SiO$_2$ NPs as calculated from their histogram is 234 ± 105 nm (Figure 2e). The current study is support by Tian et al. and Jeon et al., who synthesized Ag-SiO$_2$ NCs with an average particle size between 150 and 300 nm.[46,47] The size evaluated with the SEM analysis is greater than the crystalline size calculated from XRD. This is due to the fact that the grain/particle is the result of agglomeration of the number of nanocrystals.

Figure 2c shows the formation of randomly shaped ZnO-SiO$_2$ NPs, sometimes appearing as rectangles. The average grain/particle size was determined to be 192 ± 84 nm, as shown in Figure 2f. In the literature, such ZnO-SiO$_2$ NPs showed great antibacterial activity against many pathogens and photocatalytic properties due to their large surface areas. Our study is consistent with previous studies on such kinds of NPs.[48,49]

2.3. Optical Properties of Silica and Silica-Based Nanoparticles. The UV−Vis absorption spectrum of C-SiO$_2$ NPs is shown in Figure 3 (green). It showed a continuous absorption band with the maximum absorption between 200 and 350 nm. Figure 3 (red) presents the UV−Vis scan of Ag-SiO$_2$ NPs. A clear absorption peak is present around 430 nm, which is due to the Mie plasmon resonance excitation from Ag NPs.[50] Figure 3 (magenta) presents the UV−Vis scan of ZnO-SiO$_2$ NPs. There is a continuous absorption band present for these NPs with the prominent absorption in the range between 380 and 480 nm. The decline in the absorption band intensity at higher wavelengths is observed and is consistent with a previous study.[40]

The results of different characterizations showed that we have successfully synthesized the silica-based NPs. Due to different confinement properties of Ag, Zn, and SiO$_2$, we observed that the prepared NPs have different sizes and morphologies when compared with each other.
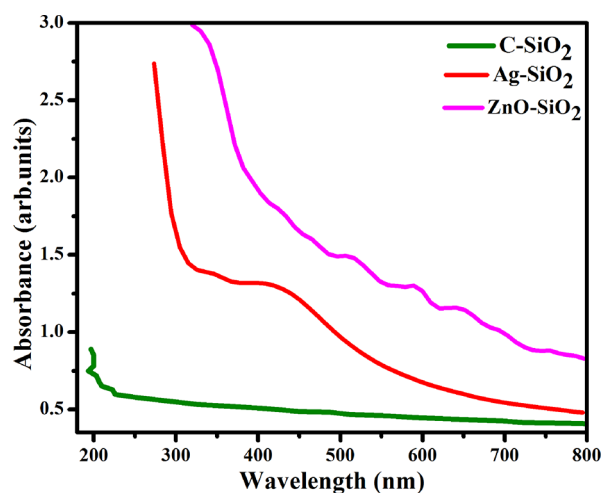

Figure 3. UV−Vis spectra of C-SiO$_2$ NPs (green), Ag-SiO$_2$ NPs (red), and ZnO-SiO$_2$ NPs (magenta).

2.4. Toxicity of Silica and Silica-Based Nanoparticles. The trail to evaluate the toxic effect of the prepared NPs spanned over 21 days, and in this, no mortality of albino rats was observed in either control or NPs-treated groups. The present study indicated that the administration of 500 μg/kg dose of ZnO-SiO$_2$, Ag-SiO$_2$, and C-SiO$_2$ NPs did not cause death in albino rats, implying that this dose might be the maximum tolerated dose and does not induce physical alterations. The mean values of the absolute and relative weight of the liver of each rat are shown in Table 1. No significant difference in the weight of NPs-treated and control albino rats was observed throughout the study. The absolute and relative weight of the liver from C-SiO$_2$ NPs-treated rats was significantly increased (Figure 4a), whereas the absolute weight of rats from ZnO-SiO$_2$ and Ag-SiO$_2$ NPs-treated groups was nonsignificantly increased when compared to the untreated group (Figure 4a). The increased relative and absolute weight of liver tissues might be related to the inflammatory reactions, hepatomegaly, and congestion in the liver. Our findings are inconsistent with Bertola who also reported changes in liver tissues.[51]

2.5. Hematological Parameters. Different blood parameters including red blood cells (RBC), hemoglobin (HGB), hematocrit (HCT), and mean corpuscular volume (MCV) of the NPs-treated rats from different groups are reported in Table 1. All these parameters were significantly ($P < 0.05$) decreased in the Ag-SiO$_2$ and C-SiO$_2$ NPs-treated groups named as C and D, respectively, whereas RBC, HGB, HCT, and MCV parameters were nonsignificantly decreased in ZnO-SiO$_2$ NPs-treated group B (Figure 4b) when compared to the unexposed group A of rats. However, the white blood cells (WBC), mean corpuscular hemoglobin concentration (MCHC), mean corpuscular hemoglobin (MCH), and neutrophil (NEUT) counts were increased in rats of groups C and D. A nonsignificant increase in these parameters was recorded in the rats of group B, as shown in Figure 4b.

In the present study, it has been observed that the rats exposed to NPs for 21 days showed elevation in WBC counts when compared to the untreated group. These results are consistent with the results of Priya et al.,[52] where they also investigated a significant increase in the percentage of total number of WBC, NEUT percentage, and MCHC in chicken and rats upon exposure to Ag-SiO$_2$ and SiO$_2$ NPs. SiO$_2$-coated ZnO NPs, on the other hand, were cleared from plasma much faster than the

Table 1. Relative and Absolute Liver Weights, Various Hematology Parameters, and Serum Biochemistry of NPs-Treated and Untreated Groups of Albino Rats[a]

	groups/treatments (500 μg/kg)			
	A	B	C	D
	control	ZnO-SiO$_2$	Ag-SiO$_2$	C-SiO$_2$
absolute liver weight	6.74 ± 0.73	6.87 ± 0.17	6.96 ± 0.49	7.25 ± 0.51*
relative liver weight	3.53 ± 0.36	3.67 ± 0.30	4.23 ± 0.31*	4.30 ± 0.39*
hematological parameters				
RBC (×10^6/mm^3)	5.93 ± 0.68	4.57 ± 0.26	3.64 ± 0.17*	2.94 ± 0.45*
HGB (g/dL)	14.01 ± 0.73	12.31 ± 0.51	11.77 ± 0.19	10.91 ± 0.73*
WBC (×10^6/mm^3)	15.19 ± 0.28	16.19 ± 0.56	17.46 ± 0.23*	18.6 ± 0.39*
HCT	49.5 ± 0.78	45.5 ± 0.31	43.4 ± 0.46*	41.1 ± 0.58*
MCH (pg)	18.9 ± 0.46	20.5 ± 0.49	21.2 ± 0.23*	22.8 ± 0.19*
MCHC (g/dL)	37.16 ± 0.78	40.41 ± 1.42	44.40 ± 3.20*	45.2 ± 1.58*
LYM (%)	7.23 ± 0.40	6.27 ± 0.36	4.71 ± 0.24*	3.86 ± 0.30*
NEUT (%)	18.1 ± 0.66	22.16 ± 0.85	23.6 ± 0.83	25.8 ± 1.06*
MCV (fL)	54.3 ± 0.56	52.3 ± 0.52	50.7 ± 0.47	48.6 ± 0.35*
serum biochemistry				
ALP (U/L)	50.3 ± 3.00	57.9 ± 2.04	63.6 ± 2.19*	68.7 ± 2.29*
ALT (U/L)	72.7 ± 6.36	76.7 ± 2.69	88.9 ± 5.08*	95.7 ± 3.40*
AST (U/L)	44.9 ± 4.46	60.4 ± 1.72*	72.3 ± 4.16*	82.3 ± 3.80*
ALB (mg/dL)	4.41 ± 0.20	3.80 ± 0.22	2.74 ± 0.16*	2.64 ± 0.17*

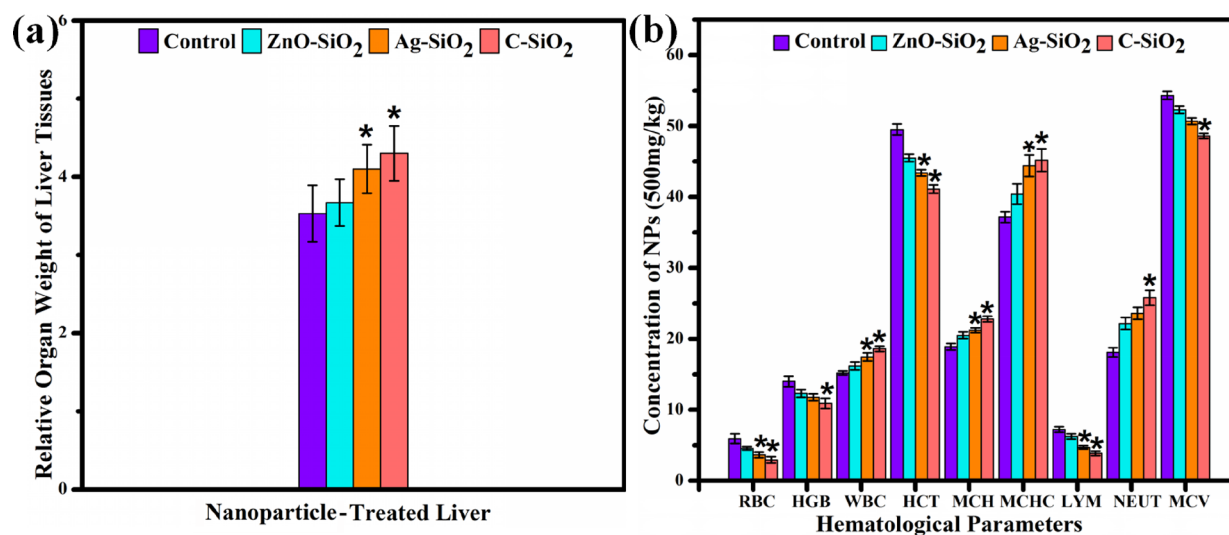[a]"*" indicates a significant increase or decrease.

Figure 4. (a) Relative organ weight profile of the liver from rats. (b) Alteration in hematological parameters (The asterisk "*" shows the significant change in liver tissues of NPs-treated groups in comparison to the control group).

uncoated ZnO NPs and became more associated with RBCs.[53] Erythrocytes are the most common cell type in blood tissue that plays an important role in the transportation of oxygen. These cells are particularly susceptible to toxicity, and oxidative stress leads to the induction of various deformities in their shape and size, hemolysis, and mitochondrial dysfunctions. Earlier studies suggested that the reduction in MCV and elevation in MCHC could be due to defensive reaction against various NPs or due to the decrease in RBC, HGB, and HCT values following the conflicts between the metabolic and hemopoietin system.[54] Our findings are also consistent with the results of Almansour et al.,[55] where elevation in WBC due to SiO$_2$ NPs due to chronic hepatotoxicity has been reported. Cook et al. described that the alterations in hematology parameters caused different ailments such as anemia and iron deficiency in different animals.[56] Furthermore, few reports on hematology parameters in other

vertebrates (albino mice, rats, and adult cockerels) exposed to toxicants are available in the literature.[57,58] The present study indicated that the Ag-SiO$_2$ and ZnO-SiO$_2$ NPs produced less alteration in the hematology parameters when compared with C-SiO$_2$ NPs and our results are in agreement with the study of Das et al., where it has been shown that coating SiO$_2$ NPs on Ag prevented the formation of Ag$^+$ ions and reduced its toxicity.[59] It has been well established that the parameters of the blood are the best biomarkers for assessing the pathophysiological status of various living organisms exposed to any toxicants and the changes in hematological values might be due to the toxic effect on the hematopoietic system. In our study, increased population of WBCs might be related to the induction of oxidative stress, leading to free radical-related injuries in rats. Previously, it has been shown that the decrease in the WBC count is due to weakening of the immune system, hence making the organisms
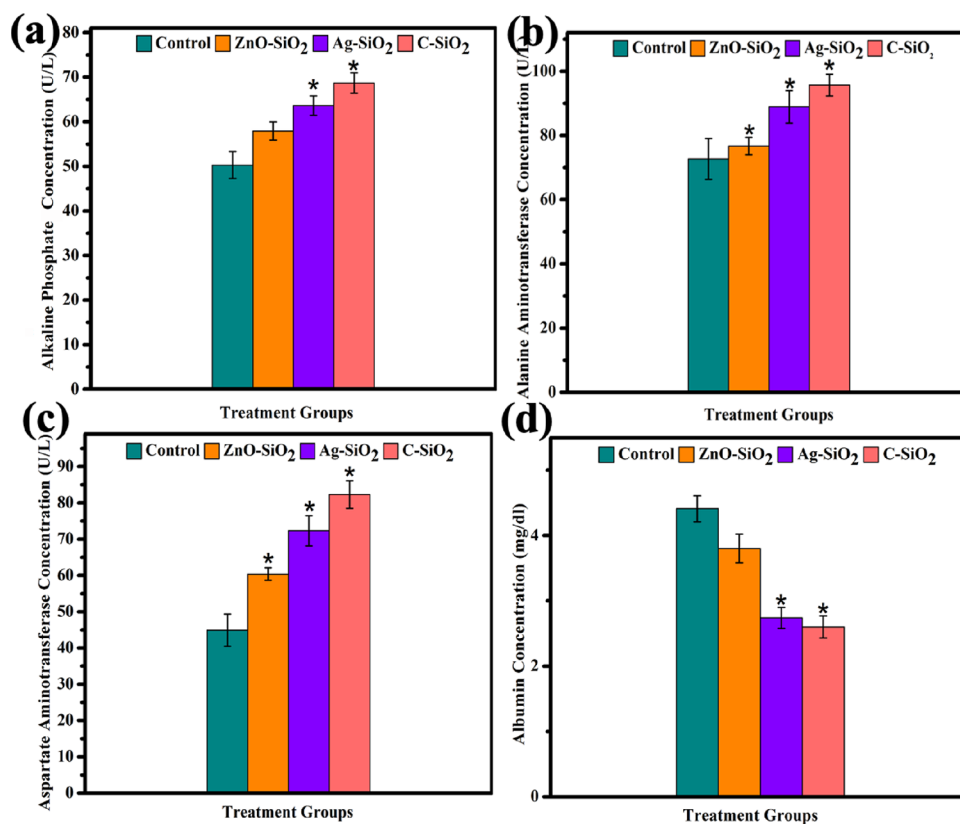
Figure 5. Comparison of various serum parameters between NPs-treated and untreated groups: (a) alkaline phosphates, (b) alanine aminotransferase, (c) aspartate aminotransferase, and (d) albumin.
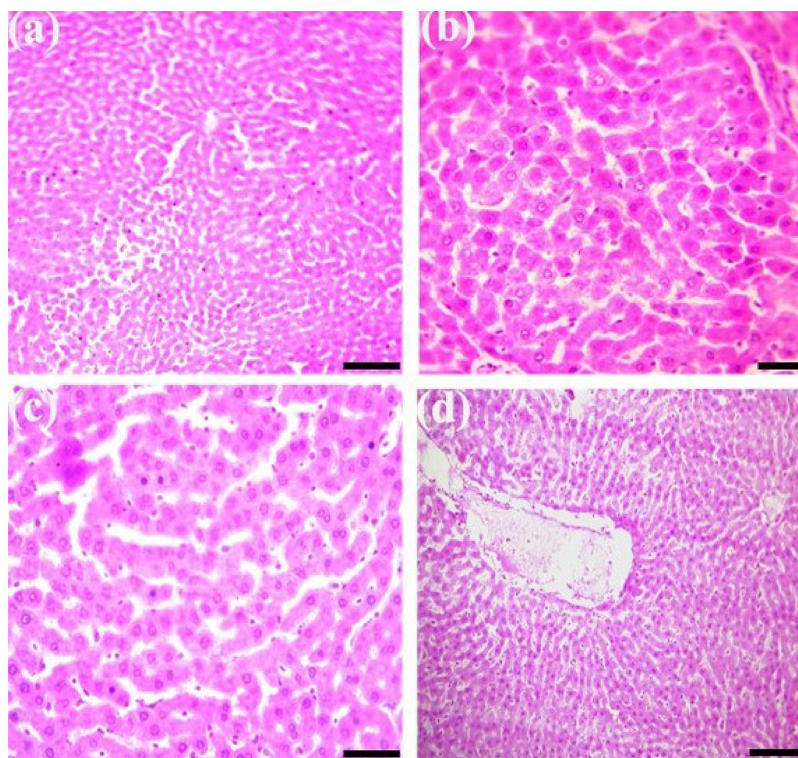

Figure 6. Photomicrograph showing different pathological alterations in the liver of NPs-treated and untreated rats. (a) Liver showing normal histoarchitecture of hepatocytes in the untreated group. (b) Mild to moderate alterations such as degeneration of hepatocytes, pyknosis, and atrophy of hepatocytes in group B. (c) Moderate to severe histological changes like necrosis of hepatocytes, atrophy of nuclei in hepatocytes, and hypertrophy of cytoplasm in group C. (d) Severe to very severe microscopic ailments such as edema, necrosis of hepatocytes, atrophy of hepatocytes, and hypertrophy of cytoplasm in group D. H & E stain; 400×.

susceptible to infections; also reported are the decreased hematological parameters in rats.[60]

2.6. Analysis of Serum Biochemistry. Various serum biochemical biomarkers are also summarized in Table 1. The liver biomarkers such as aspartate aminotransferase (AST), alanine aminotransferase (ALT), and alkaline phosphates (ALP) in the NPs-treated rats were significantly increased in groups C and D, whereas the quantity of albumin (ALB) was significantly decreased in both groups when compared with the unexposed groups A. AST, ALT, and ALP were nonsignificantly increased in rats of group B, and ALB was nonsignificantly reduced in group B (Figure 5a−d). Alteration in blood biomarkers in NPs-treated groups could be attributed to toxic effects resulting from the over generation of free radicals, leading to induction of oxidative stress.

The liver is the major organ of the body that helps in removing and circulating macromolecules and microorganisms through the hepatic reticuloendothelial system. In the present study, the increased values of biomarkers (ALT, AST, and ALP) in the liver of rats could be linked to the higher levels of oxido-nitrosative stress, causing an increased level of hepatotoxicity. Our study demonstrated that severity of serum parameter alterations was more prominent in rats exposed to C-SiO$_2$ followed by Ag-SiO$_2$ NPs and ZnO-SiO$_2$ NPs (Figure 5a−d). C-SiO$_2$ NPs are thought to be able to penetrate the bloodstream and localize in the liver tissue, causing more oxidative stress and changes in the liver enzymatic concentration than ZnO-SiO$_2$ and Ag-SiO$_2$ nanocomposites. Our results are in agreement with the study of Sun et al.[61] where they reported that an intratracheal instillation of SiO$_2$ NPs caused hepatic dysfunction as evidenced by various pathological changes in the liver tissue and a clear increase in ALT and AST concentrations. Our findings are also consistent with the recent study that found hepatotoxicity in male rats and altered renal functions as evidenced by elevated liver enzymatic activities. The significantly lower serum mineral contents can be attributed to abnormal physiological changes caused by oxidative stress, resulting in poor absorption and bioavailability in infected rats. The alterations in the liver of NPs-treated rats could also be related to dysfunctions of mitochondrial hepatocytes. Furthermore, earlier research has found that an increase in AST, ALP, ALT, and lipid peroxidation (LPO) could be caused by hepatic degeneration, oxidative stress, and hypoxic conditions of various tissues in the body.[61] The elevation in ALP concentration might be due to the abnormalities in the liver tissues, gall bladder, or bones.

2.7. Microscopic Histopathological Examination. Microscopic investigations of liver tissues from the control group A of rats indicated normal functions. Untreated rats showed normal hepatic arrangements including lobule structure, components of the portal hepatic space, and hepatocytes (Figure 6a−d). Although different histopathological disorders were examined in the liver of rats exposed to NPs, at the gross level, the liver tissues appeared fatty, friable, and pale yellow in color. At the microscopic level, necrosis and hemorrhages were observed in the liver of all three NPs-exposed groups. The liver tissues (Figure 6d) of rats from group D exhibit very severe ailments such as edema, necrosis of hepatocytes, atrophy and karyorrhexis of hepatocytes, pyknosis, and hypertrophy of cytoplasm. Meanwhile, moderate alterations such as degeneration of hepatocytes, pyknosis, and atrophy of hepatocytes were observed on group B (Figure 6b) and severe histological changes like necrosis of hepatocytes, atrophy of the nuclei of hepatocyte, and hypertrophy of cytoplasm were observed in group C (Figure

6c). Different histopathological lesions like necrosis of hepatocytes, congestion, edema, atrophy, degeneration of hepatocytes, and ceroid information were examined in the liver tissues of the NPs-exposed groups. The severity of these lesions was changed from moderate to very severe, as recorded in Table 2. Very severe histopathological lesions were observed

Table 2. Severity of Histopathological Lesions in the Liver Tissue of Albino Rats Exposed to NPs[a]

| | group/treatments (500 μg/kg) | | | |
| | A | B | C | D |
histopathological lesions in liver	control	ZnO-SiO$_2$	Ag-SiO$_2$	C-SiO$_2$
vacuolar degeneration	−	++	+++	++++
congestion	−	+	+++	++++
pyknosis	−	++	++	++++
karyolysis	−	++	+++	++++
degeneration of hepatocyte	−	+	++	++++
nuclear hypertrophy	−	++	+++	++++
karyorrhexis	−	++	++++	++++
necrosis of hepatocytes	−	++	+++	++++
atrophy of hepatocyte	−	+	++	++++
hepatocytes with eccentric nuclei	−	++	+++	++++
hemorrhages	−	++	+++	++++
ceroid formation	−	++	+++	++++

[a]Absent (−); mild (+); moderate (++); severe (+++); very severe (++++).

in rats of group D, whereas moderate to severe lesions were observed in rats of group C (Figure 6c) and mild to moderate in rats of group B (Figure 6b and Table 2). According to our findings, the histopathological changes in liver tissue are caused by the rapid and increased creation of oxidative stress. Fan et al.[62] indicated that the accumulation of prepared NPs may cause histopathological changes in the liver. Several histological ailments in the liver (increased liver weight, hepatic lobules, portal triads, hydropic degeneration, karyolysis, fatty degeneration of hepatocyte, sinusoidal dilatation, and pyknosis) have been investigated in rats and chickens treated with different sizes of SiO$_2$ and SiO$_2$-based NPs.[63]

Our findings showed that the ZnO-SiO$_2$, Ag-SiO$_2$, and C-SiO$_2$ NPs can induce histopathological alterations in the liver. All these observations suggest liver injuries in albino rats treated with NPs. These findings pointed out that the liver was the target organ for SiO$_2$ NPs. A few of these discoveries are consistent with the earlier literature related to the histopathological changes caused by SiO$_2$ NPs in human liver tissues.[64] Previously, it was recorded that the SiO$_2$ nanorattles caused histopathological changes in multiple organs of mice including vacuolar degeneration in hepatocytes and the blockage of central vein, indicating that cytoplasmic injury is a type of hydropic degeneration that causes necrosis and degradation of cellular organelles.[63,65]

Necrosis is frequently caused by toxins that affect the nucleus, endoplasmic reticulum, and cytoplasmic membranes. According to our findings, C-SiO$_2$ causes more hepatotoxicity in the liver when compared to ZnO-SiO$_2$ and Ag-SiO$_2$ NPs. Almansour et al. discovered similar results stating that the intraperitoneal administration of SiO$_2$ (2 mg/kg body weight) may alter hepatocellular protein synthesis.

2.8. Oxidative and Antioxidant Enzymes in the Liver and Erythrocytes. The reactive oxygen species (ROS) and thiobarbituric acid reactive substances (TBARS) in the liver of

Table 3. Status of Oxidative and Antioxidant Parameters in the Liver of Untreated and NPs-Treated Albino Rats

| | groups/treatments (500 μg/kg) | | | |
| | A | B | C | D |
parameters	control	ZnO-SiO$_2$	Ag-SiO$_2$	C-SiO$_2$
oxidative enzymes				
ROS (optical density)	0.20 ± 0.02	0.27 ± 0.03	0.35 ± 0.04*	0.47 ± 0.05*
TBARS (nmol/TBARS formed/mg protein/min)	0.30 ± 0.02	0.36 ± 0.02	0.41 ± 0.03*	0.48 ± 0.04*
GSH (mmol-g^{-1} tissue)	0.65 ± 0.04	0.34 ± 0.03*	0.28 ± 0.02*	0.22 ± 0.01*
antioxidant enzymes				
catalase(units/min)	0.97 ± 0.08	0.89 ± 0.06	0.57 ± 0.04*	0.49 ± 0.02*
peroxidase (units/min)	0.70 ± 0.09	0.34 ± 0.04	0.25 ± 0.03*	0.16 ± 0.02*
superoxide (units/mg protein)	0.41 ± 0.06	0.33 ± 0.05	0.28 ± 0.04*	0.14 ± 0.03*

Table 4. Status of Oxidative and Antioxidant Parameters in Erythrocytes (RBCs) of Untreated and Treated (ZnO-SiO$_2$, AgSiO$_2$, and C-SiO$_2$ NPs) Albino Rats[a]

| | groups/treatments (500 μg/kg) | | | |
| | A | B | C | D |
parameters	control	ZnO-SiO$_2$	Ag-SiO$_2$	C-SiO$_2$
oxidative enzymes				
ROS (optical density)	0.16 ± 0.01	0.24 ± 0.03*	0.43 ± 0.05*	0.56 ± 0.03*
TBARS (nmol/TBARS formed/mg protein/min)	0.24 ± 0.01	0.28 ± 0.02	0.37 ± 0.02*	0.48 ± 0.10*
GSH (mmol-g^{-1} tissue)	1.58 ± 0.17	0.91 ± 0.37*	0.88 ± 0.04*	0.69 ± 0.06*
antioxidant enzymes				
catalase (units/min)	0.82 ± 0.06	0.76 ± 0.03	0.47 ± 0.03*	0.27 ± 0.02*
peroxidase (units/min)	0.20 ± 0.03	0.15 ± 0.01	0.12 ± 0.01*	0.11 ± 0.02*
superoxide (units/mg protein)	0.68 ± 0.08	0.36 ± 0.02*	0.26 ± 0.03*	0.18 ± 0.04*

[a]"*" indicates a significant increase and decrease.

NPs-treated rat were increased significantly in groups C and D, whereas these biomarkers were increased nonsignificantly in group B when compared with untreated rats (Table 3). Glutathione (GSH) and different other antioxidant enzymes including catalase (CAT), peroxidase (POD), and superoxide dismutase (SOD) decreased significantly in the liver tissues of NPs-exposed rats in groups C and D; however, GSH and all antioxidant enzymes in group B decreased nonsignificantly when compared with the unexposed rats (Table 3).

The results indicated that GSH and SOD were reduced significantly in erythrocytes of NPs-treated groups B, C, and D. However, POD and CAT were significantly decreased in erythrocytes of groups C and D, while these biomarkers were nonsignificantly decreased in group B. The oxidative stress biomarkers showed significantly higher quantity of ROS and TBARS in erythrocytes of NPs-exposed rats in groups C and D, whereas ROS and TBARS in the erythrocytes of group B increase nonsignificantly when compared with the unexposed rats (Table 4).

An imbalance between radical-generating and radical-scavenging systems causes oxidative stress, which leads to cell membrane impairment and DNA damage. Based on antioxidant activities, our study predicted the occurrence of imbalance in oxidant enzymes that induced the inflammatory response, as evidenced by a clear reduction in the levels of antioxidant enzymes (POD, SOD, and CAT) and oxidative enzyme (GSH) in the liver and blood tissue of rats and an increase in oxidative biomarkers (TBARS and ROS). Liu et al.[66] discovered similar results, reporting that the SiO$_2$ NPs can cause cytotoxicity in the liver of mice via an inflammatory response and oxidative stress. Our findings contradict with those of Nemmar et al.,[67] which reported an increase in antioxidant enzymes, indicating the

oxidative stress caused by amorphous SiO$_2$ NPs in mice accompanied with an increase in SOD and CAT activities.[68] Our findings indicated that SiO$_2$ NPs cause a significant and nonsignificant increase in LPO in the liver and blood. The NPs induction in the liver increased the number of cells with damaged DNA. According to our findings, oxidative stress is caused by an increase in the amount of ROS and TBARS in the liver and erythrocytes of NPs-exposed rats. A similar study found oxidative stress in the liver after IV administration of amorphous SiO$_2$ NPs in rats.[65,69−71] There is no data available in the literature on Zn-SiO$_2$- and Ag-SiO$_2$-induced oxidative stresses in the albino rat's liver and blood. However, detoxifying systems of rats, being exposed to different toxicants, cause the fast and increase formation of ROS. This production initiates the LPO process, causing cellular membrane irregularities and the formation of TBARS. According to the findings of the present study, an increase in the quantity of oxidative stress biomarkers in NPs-treated rats may be linked to the depletion of antioxidant enzymes. The decrease in CAT reported in the liver, on the other hand, suggests that it is consumed during the breakdown of free radicals. CAT is the key enzyme involved in cellular defense against oxidative stress.[72−74] This study demonstrated that the deposition of C-SiO$_2$ NPs increased the TBARS quantity and reduction in SOD and GSH activities in the liver of rats, indicating an increase in ROS production and oxidative stress. The production of H$_2$O$_2$ and SOD ion radicals from isolated electron transport chains is a well-known process.[75] The most prevalent ROS is hydrogen peroxide.[65] SiO$_2$ NPs cause ROS generation and oxidative damage due to unsaturated bonds and a silicon-bounded hydroxyl group on the particle surface. The present study is supported by the previous findings that the increase in GSH activities causes oxidative damage in the liver

and erythrocytes when exposed to amorphous SiO_2 NPs.[67] The previous literature focused on hematology, histopathology, and serum biomarkers as tools of judgment of injuries to various organs. However, our current findings are innovative and provide insights into the mechanisms underlying organ toxicity caused by $C-SiO_2$, $Ag-SiO_2$, and $ZnO-SiO_2$ NPs. In this study, the significant and nonsignificant elevation and reduction in oxidative and antioxidant enzymes occur in the following manner: $C-SiO_2 > Ag-SiO_2 > ZnO-SiO_2$.

3. EXPERIMENTAL SECTION

For the preparation of NPs, commercially available chemicals including tetraethyl orthosilicate (TEOS) $[Si(OC_2H_5)_4]$, zinc acetate $[Zn(CH_3CO_2)2 \cdot 2H_2O]$, silver acetate $[AgC_2H_3O_2]$, ammonia $[NH_3]$, ethylene glycol $[CH_2OH]$, ethanol $[CH_3CH_2OH]$, sodium hydroxide $[NaOH]$, and hydrochloric acid $[HCl]$ were used. Distilled and deionized water was used throughout the experiment.

3.1. Synthesis of $C-SiO_2$, $Ag-SiO_2$, and $ZnO-SiO_2$ NPs. For the synthesis of $C-SiO_2$, first, 30 mL of ethanol was mixed with 90 mL of ammonia and named as solution A. Second, 0.5 mL of TEOS was added in 7 mL of distilled water and named as solution B. Here, TEOS will act as a precursor medium for SiO_2. Later, the solution B was added drop by drop to the solution A. This mixture was centrifuged (Hettich-EBA 20-) at 3000 rpm for 10 min, cleaned with distilled water, and then dried to produce amorphous SiO_2 NPs. These amorphous SiO_2 NPs were later placed in a furnace (Ney VULCAN D-550) for 1 h at 1100 °C to obtain the $C-SiO_2$ NPs.

For the synthesis of nanocomposites, 100 mL of TEOS was mixed with 200 mL of ethanol, 42 mL of water was added dropwise, and the solution was named as solution C. Later, 100 mL of ethylene glycol was mixed with 1 g of silver acetate and separately 100 mL with 1 g of zinc acetate. Both the solutions were transferred into separate flasks with refluxing arrangement. These solutions were then heated continuously for 4 h between the temperature ranges of 100−120 °C. After cooling down the solutions at room temperature, the precipitated material was removed and shift into another pot and mixed with 40 mL of acetone to wash out the solutions. The washing procedure was repeated three to four times, and then the samples were dried. The final products were Ag and ZnO NPs and were identified as solutions D and E, respectively. Later, the solution C was added dropwise with continuous stirring into the solutions D and E. Ammonia was utilized to precipitate the prepared solutions, which were then filtrated using filter paper to eliminate residual ammonium hydroxide and unreacted TEOS. Precipitates were washed several times with an excess amount of water. The final products were the nanocomposites named as $Ag-SiO_2$ and $ZnO-SiO_2$ NPs.

3.2. Sample Characterizations. To confirm the formation of desired NPs, different characterization techniques were employed. UV−Vis spectrometry (EPOCH-BIO TECK, USA) was performed in the wavelength range 200−800 nm at a resolution of 1 nm to observe the light absorption pattern for the three NPs. The NPs were dissolved in normal saline for absorption spectroscopy. FTIR (SRUKER TENSOR 27) was performed to look for the functional groups associated with the formation of NPs. FTIR analysis of all prepared samples was performed in the range of 400−4000 cm^{-1} at a resolution of 4 cm^{-1} by converting the air-dried powder of NPs into pellets. Powdered XRD (D8 DISCOVER-Bruker) was done to confirm the nature (crystalline or amorphous) and structure of the NPs.

The diffraction patterns of the NPs were obtained on 40 kV voltage and 30 mA current settings at 0.2 s per count with 20−80° scanning range utilizing Cu X-rays. The obtained XRD patterns were compared with the standard JCPDS cards for the confirmation of the desired material.

3.3. Animal Management. Twenty-six mature albino rats were used for the biological evaluation of NPs. Thirteen male and thirteen female albino rats weighing between 100 and 160 g were kept for 21 days in different groups. The rats were obtained from National Laboratory Animal Center Lahore, Pakistan. Throughout the trail, the experimental rats were free from any kind of disease and had free access to food and clean tap water. Animals were housed in steel cages, with the male and female rats in separate cages. The cages were subjected to a 12 h light−dark cycle at a temperature of 26 ± 2 °C and a constant humidity of $65 \pm 4\%$. The cages were regularly cleaned to maintain hygienic conditions. The rats were acclimatized for few weeks prior to the start of experimental study. All the research and experimentations were carried out with the prior approval from the university's ethical committee and in accordance with the National Institute of Health's "Guide for the Care and Use of Laboratory Animals" (NIH publication np.85-23.1985).

3.4. Toxicology Profile. Twenty-six rats were randomly distributed in four groups (A−D). Male and female rats were present in separate groups. The first group (A) served as the controlled one and was fed only with normal food and clean water. The rats of the remaining three groups B, C, and D received a dose of 500 μg/kg body weight of $ZnO-SiO_2$, $Ag-SiO_2$, and $C-SiO_2$ NPs, respectively, via IV route every third day. The duration of this trial was 21 days. After 21 days of the trial, blood was collected from the jugular vein of each rat and was collected in two types of tubes. The blood collected in an anticoagulated tube with ethylenediaminetetraacetic acid (EDTA) was immediately used for blood biochemical analysis. The blood collected in tubes without EDTA was centrifuged in a refrigerated centrifuge machine at 4000 rpm at 4 °C for 15 min to obtain plasma for the analysis of serum parameters.

3.5. Clinical Signs, Body Weight, and Feed Intake. The body weight and feed intake were recorded on a daily basis. Different physical disorders like drowsiness, diarrhea, anorexia, abnormal posture, and other behavioral changes were also observed on a daily basis.

3.6. Serum Parameters. Biochemical analysis of serum was performed using standard laboratory techniques and a chemistry analyzer (MAX Company). Serum parameters including ALP, ALT, AST, and ALB were evaluated to monitor the liver functions.

3.7. Hematology Parameters. The hematological profile was evaluated utilizing an automated hematology analyzer. About 2 mL of blood was collected in EDTA tubes from each rat of NPs-treated and untreated groups. RBC counts, WBC counts, HGB, (HCT)/PCV, MCH, MCHC, MCV, and NEUT were analyzed. RBC, HGB, and HCT are used as biomarkers of anemia and reflect the efficiency of blood forming tissues (hematopoietic tissues). MCV reflects the size of the RBCs. These hematological parameters were immediately measured on the sampling day within 1 h after blood collection.

3.8. Histopathological Evaluation. Livers from NPs-treated and untreated rats were removed on the sampling day and placed on absorbent papers for few minutes. Later, the absolute weight of each sample was calculated in grams. The relative liver weight (RLW) of NPs-treated and untreated groups was calculated[76] as follows:

relative liver weight (RLW)

$$= \left[\frac{\text{absolute liver weight in g}}{\text{bodyweight of rats on sampling day in g}} \right] \times 100$$

(2)

Tissues from each organ were then fixed in 10% formalin solution and were routinely examined using the traditional paraffin embedding techniques described earlier.[77] In brief, a 4—5 μm-thick piece of liver from each group of rats was sectioned using microtome, dehydrated, embedded in paraffin wax, and stained with hematoxylin and eosin stains. All the processed sections were carefully observed by an experienced pathologist for the determination of NPs-related hepatotoxicity. Representative photomicrophages were obtained with a digital camera.

3.9. Tissue Preparation and Biochemical Analyses. The erythrocytes and livers were taken from each NPs-treated and untreated albino rats for the determination of oxidative and antioxidant enzymes. In brief, 100 mg of liver tissue was taken from each rat. All the tissues were minced and homogenized separately in a Petri plate containing 2 mL ice-cold normal saline solution. The homogenates were separately centrifuged (Hettch-EBA 20-) at 4000 rpm for 5 min, and the supernatant was collected from each triturated sample and preserved at 20 °C for further studies. Furthermore, biochemical parameters were estimated in 10% hemolysate of RBC. Briefly, blood samples were centrifuged at 4000 rpm for 10 min, plasma was separated, and pellets containing RBC were collected. Later on, all the blood samples were treated with 0.3 mL of normal saline solution to get 10% hemolysate. Oxidative stress biomarkers such as ROS, TBARS, and reduced GSH in the livers and erythrocytes of the NPs-treated and untreated rats were determined at 505, 532, and 412 nm by utilizing a UV—Vis spectrophotometer. At least four readings were taken at the interval of 15 s. At 470, 560, and 240 nm, different antioxidant parameters such as POD, SOD, and CAT were also measured in the liver and erythrocytes.

3.10. Statistical Analysis. $P \leq 0.05$ was set as a significant level. The data obtained from the hematology profile, serum profile, oxidative stress, and antioxidant enzymes was analyzed by utilizing the analysis of variance (ANOVA) and Post-Hoc test using IBM SPSS for Windows version 8.1. Collected data was represented as mean $\pm$ S.E. for all studied parameters of complete blood count, serum biochemistry, and oxidative and antioxidant enzymes for NPs-treated and untreated groups.

4. CONCLUSIONS

As the utilization of NPs is increasing day by day, this increase leads to elevated release of these NPs into the environment and the living organisms that are in contact with these NPs. To study the biological effects, C-SiO$_2$, Ag-SiO$_2$, and ZnO-SiO$_2$ NPs were prepared by the sol—gel and co-precipitation techniques. XRD, FTIR, and UV—Vis absorption confirmed the formation of NPs. From XRD data analysis, crystallite sizes for all the prepared NPs were evaluated and all three of them showed different sizes due to the different confinement properties of materials under the synthesis process. The particle/grain sizes evaluated by SEM analysis showed large sized NPs as a result of agglomeration of NPs. The present study investigated the effect of C-SiO$_2$, Ag-SiO$_2$, and ZnO-SiO$_2$ NPs on bodyweight, hematological, serological, histopathological, and oxidative and antioxidant enzymes in albino rats. These evaluated parameters could serve as a valuable biomarker in monitoring nanotoxicology and

environmental changes. The C-SiO$_2$ NPs exhibit more toxic results when compared to the Ag-SiO$_2$ and ZnO-SiO$_2$ nanocomposites. The results of the current study pointed out the need for the safe disposal of NPs and development of proper protocols to be followed while using these NPs for different applications. Here, we would like to add that further study on the toxicity based on NPs size distribution is required to understand more about the toxic effect of NPs. More size-controlled synthesis of NPs is also required.

■ ASSOCIATED CONTENT

ⓈI Supporting Information

The Supporting Information is available free of charge at https://pubs.acs.org/doi/10.1021/acsomega.3c01674.

(Figure S1) Images of body weight measurement of rats, blood collection, transfer of blood into EDTA tubes, dissected rat at day 22 after the trail period, and visceral organs of rats collected; (Figure S2) absolute weight of the liver (PDF)

■ AUTHOR INFORMATION

Corresponding Authors

Saba Saeed — *Institute of Physics, Faculty of Physical & Mathematical Sciences, The Islamia University of Bahawalpur, Bahawalpur, Punjab 63100, Pakistan*; Email: saba.saeed@iub.edu.pk

Murtaza Hasan — *Department of Biotechnology, Faculty of Chemical & Biological Sciences, The Islamia University of Bahawalpur, Bahawalpur, Punjab 63100, Pakistan; College of Chemistry and Chemical Engineering, Zhongkai University of Agriculture and Engineering, Guangzhou 510225, China;* ⓞ orcid.org/0000-0001-7715-9173; Phone: 86-020-8900-3114; Email: murtaza@zhku.edu.cn

Giovanni Caprioli — *Chemistry Interdisciplinary Project (CHip), School of Pharmacy, University of Camerino, Camerino 62032, Italy;* ⓞ orcid.org/0000-0002-5530-877X; Email: giovanni.caprioli@unicam.it

Authors

Arooj Ali — *Institute of Physics, Faculty of Physical & Mathematical Sciences, The Islamia University of Bahawalpur, Bahawalpur, Punjab 63100, Pakistan*

Riaz Hussain — *Department of Pathology, Faculty of Veterinary & Animal Sciences, The Islamia University of Bahawalpur, Bahawalpur, Punjab 63100, Pakistan*

Gulnaz Afzal — *Department of Zoology, Faculty of Chemical & Biological Sciences, The Islamia University of Bahawalpur, Bahawalpur, Punjab 63100, Pakistan*

Abu Baker Siddique — *Department of Microbiology, Faculty of Life Sciences, Government College University, Faisalabad, Punjab 38000, Pakistan*

Gulnaz Parveen — *Department of Botany, Faculty of Science, Women University Swabi, Swabi, Khyber Pakhtunkhwa 23430, Pakistan*

Complete contact information is available at:
https://pubs.acs.org/10.1021/acsomega.3c01674

Author Contributions

A.A. performed the measurements; S.S. and R.H. were responsible for the planning and supervised the work. A.A., S.S., and R.H. processed the experimental data, performed the analysis, drafted the manuscript, and designed the figures. G.A.,

A.B.S., and G.P. were involved in the interpretation of results. M.H. and G.C. supervised and helped in finalizing the manuscript.

Notes

■ ACKNOWLEDGMENTS

■ REFERENCES

(1) Wu, Z.; et al. Synthesis, characterization, immune regulation, and antioxidative assessment of yeast-derived selenium nanoparticles in cyclophosphamide-induced rats. *ACS Omega* **2021**, *6*, 24585−24594.

(2) Luo, F.; et al. Synthesis of zinc oxide eudragit FS30D nanohybrids: structure, characterization, and their application as an intestinal drug delivery system. *ACS Omega* **2020**, *5*, 11799−11808.

(3) Awan, M. U. F.; et al. Neuroprotective role of BNIP3 under oxidative stress through autophagy in neuroblastoma cells. *Mol. Biol. Rep.* **2014**, *41*, 5729−5734.

(4) Yang, Y.; Qin, Z.; Zeng, W.; Yang, T.; Cao, Y.; Mei, C.; Kuang, Y. Toxicity assessment of nanoparticles in various systems and organs. *Nanotechnol Rev* **2017**, *6*, 279−289.

(5) Akram, I. N.; et al. Synthesis, characterization, and biocompatibility of lanthanum titanate nanoparticles in albino mice in a sex-specific manner. *Naunyn-Schmiedeberg's Arch. Pharmacol.* **2020**, *393*, 1089−1101.

(6) Salama, D. M.; et al. Effect of zinc oxide nanoparticles on the growth, genomic DNA, production and the quality of common dry bean (Phaseolus vulgaris). *Biocatalysis and Agricultural Biotechnology* **2019**, *18*, No. 101083.

(7) Milla, L.; et al. Monitoring of honey bee floral resources with pollen DNA metabarcoding as a complementary tool to vegetation surveys. *Ecological Solutions and Evidence* **2022**, *3*, No. e12120.

(8) Hashemi, D.; et al. Design principles for the energy level tuning in donor/acceptor conjugated polymers. *Phys. Chem. Chem. Phys.* **2019**, *21*, 789−799.

(9) Hasan, M.; et al. Biocompatibility of iron carbide and detection of metals ions signaling proteomic analysis via HPLC/ESI-Orbitrap. *Nano Res.* **2017**, *10*, 1912−1923.

(10) Rastogi, A.; Zivcak, M.; Sytar, Q.; Kalaji, HM; He, X.; Mbarki, S.; Brestic, Met al., 2017.

(11) Charehgani, H.; Fakharzadeh, S.; Nazaran, M. H. Evaluation of nano-chelated silicon fertilizer in the management of Meloidogyne javanica in tomato. *Indian Phytopathology* **2021**, *74*, 1027−1034.

(12) Mariz-Ponte, N.; et al. Silicon titanium oxide nanoparticles can stimulate plant growth and the photosynthetic pigments on lettuce crop. *Agriculture (Pol'nohospodárstvo)* **2020**, *66*, 148−160.

(13) Sotiriou, G. A.; et al. Engineering safer-by-design silica-coated ZnO nanorods with reduced DNA damage potential. *Environ. Sci.: Nano* **2014**, *1*, 144−153.

(14) Huang, R.; et al. Mesoporous silica nanoparticles: Facile surface functionalization and versatile biomedical applications in oncology. *Acta Biomater.* **2020**, *116*, 1−15.

(15) El-Naggar, M. E.; et al. Surface modification of SiO2 coated ZnO nanoparticles for multifunctional cotton fabrics. *J. Colloid Interface Sci.* **2017**, *498*, 413−422.

(16) Milić, M.; et al. Response of platelets to silver nanoparticles designed with different surface functionalization. *J. Inorg. Biochem.* **2021**, *224*, No. 111565.

(17) Huang, L.; et al. Synthesis of phytonic silver nanoparticles as bacterial and ATP energy silencer. *J. Inorg. Biochem.* **2022**, *231*, No. 111802.

(18) UshaVipinachandran, V.; et al. Citrate capped silver nanoparticles as an instantaneous colorimetric selective sensor for neomycin and thiamine in wastewater. *New J. Chem.* **2022**, *46*, 14081−14090.

(19) Tkachenko, T.; et al. Physico-chemical properties of biogenic SiO2 nanoparticles obtained from agriculture residue. *Appl. Nanosci.* **2020**, *10*, 4617−4623.

(20) El Messaoudi, N.; et al. Biosynthesis of SiO2 nanoparticles using extract of Nerium oleander leaves for the removal of tetracycline antibiotic. *Chemosphere* **2022**, *287*, No. 132453.

(21) Hasan, M.; Teng, Z.; Iqbal, J.; Awan, U.; Meng, S.; Dai, R.; Qing, H.; Deng, Y. Assessment of bioreducing and stabilizing potential of Dragon's blood (Dracaena cochinchinensis, Lour. SC Chen) resin extract in synthesis of silver nanoparticles. *Nanosci. Nanotechnol. Lett.* **2013**, *5*, 780−784.

(22) Hasan, M.; et al. Mechanistic study of silver nanoparticle's synthesis by dragon's blood resin ethanol extract and antiradiation activity. *J. Nanosci. Nanotechnol.* **2015**, *15*, 1320−1326.

(23) Hasan, M.; Sajjad, M.; Zafar, A.; Hussain, R.; Anjum, S. I.; Zia, M.; Ihsan, Z.; Shu, X. Blueprinting morpho-anatomical episodes via green silver nanoparticles foliation. *Green Processes Synth.* **2022**, *11*, 697−708.

(24) Fatemi, H.; Esmaiel Pour, B.; Rizwan, M. Foliar application of silicon nanoparticles affected the growth, vitamin C, flavonoid, and antioxidant enzyme activities of coriander (Coriandrum sativum L.) plants grown in lead (Pb)-spiked soil. *Environ. Sci. Pollut. Res.* **2021**, *28*, 1417−1425.

(25) Cao, D.; Shu, X.; Zhu, D.; Liang, S.; Hasan, M.; Gong, S. Lipid-coated ZnO nanoparticles synthesis, characterization and cytotoxicity studies in cancer cell. *Nano Convergence* **2020**, *7*, 14−18.

(26) Hussain, R.; et al. Casting zinc oxide nanoparticles using Fagonia blend microbial arrest. *Appl. Biochem. Biotechnol.* **2023**, *195*, 264−282.

(27) Konduru, N. V.; et al. Surface modification of zinc oxide nanoparticles with amorphous silica alters their fate in the circulation. *Nanotoxicology* **2016**, *10*, 720−727.

(28) Saif, M.; Haq, A; Tariq. ul, T.; Batool, S.; Dilshad, M.; Hasan, M.; Shu, X et al., 2021.

(29) Hasan, M.; Altaf, M.; Zafar, A.; Hassan, S. G.; Ali, Z.; Mustafa, G.; Munawar, T.; Saif, M. S.; Tariq, T.; Iqbal, F.; Khan, M. W.; Mahmood, A.; Mahmood, N.; Shu, X. Bioinspired synthesis of zinc oxide nanoflowers: A surface enhanced antibacterial and harvesting efficiency. *Mater. Sci. Eng., C* **2021**, *119*, No. 111280.

(30) Manzoor, Y.; et al. Incubating Green Synthesized Iron Oxide Nanorods for Proteomics-Derived Motif Exploration: A Fusion to Deep Learning Oncogenesis. *ACS Omega* **2022**, 47996.

(31) Zafar, A.; Hasan, M.; Tariq, T.; Dai, Z. Enhancing Cancer Immunotherapeutic Efficacy with Sonotheranostic Strategies. *Bioconjugate Chem.* **2022**, *33*, 1011−1034.

(32) Zafar, A.; et al. Green-maturation of Cobalt-Oxide nano-sponges for reinforced bacterial apoptosis. *Colloid and Interface Science Communications* **2021**, *45*, No. 100531.

(33) Hasan, M.; et al. Biological entities as chemical reactors for synthesis of nanomaterials: Progress, challenges and future perspective. *Materials Today Chemistry* **2018**, *8*, 13−28.

(34) Gordon, A. T.; et al. Introduction to nanotechnology: potential applications in physical medicine and rehabilitation. *Am. J. Phys. Med. Rehab.* **2007**, *86*, 225−241.

(35) Mitter, N.; Hussey, K. Moving policy and regulation forward for nanotechnology applications in agriculture. *Nat. Nanotechnol.* **2019**, *14*, 508−510.

(36) Qasim, S.; et al. Green synthesis of iron oxide nanorods using Withania coagulans extract improved photocatalytic degradation and antimicrobial activity. *J. Photochem. Photobiol., B* **2020**, *204*, No. 111784.

(37) Raj, S.; et al. Morphology controlled Ag@ SiO 2 core−shell nanoparticles by ascorbic acid reduction. *J. Mater. Sci.: Mater. Electron.* **2014**, *25*, 1156−1161.

(38) Rodrigues, M. C.; et al. Biogenic synthesis and antimicrobial activity of silica-coated silver nanoparticles for esthetic dental applications. *Journal of Dentistry* **2020**, *96*, No. 103327.

(39) Abdel Messih, M.; et al. Facile approach to prepare ZnO@ SiO 2 nanomaterials for photocatalytic degradation of some organic pollutant models. *J. Mater. Sci.: Mater. Electron.* **2019**, *30*, 14291−14299.

(40) El-Nahhal, I. M.; et al. Synthesis & characterization of silica coated and functionalized silica coated zinc oxide nanomaterials. *Powder Technol.* **2016**, *287*, 439−446.

(41) Yuvakkumar, R.; et al. High-purity nano silica powder from rice husk using a simple chemical method. *J. Exp. Nanosci.* **2014**, *9*, 272−281.

(42) Praseptiangga, D. et al. Preparation and FTIR spectroscopic studies of SiO2-ZnO nanoparticles suspension for the development of carrageenan-based bio-nanocomposite film. in *AIP Conference Proceedings.* 2020. AIP Publishing LLC.

(43) Hussain, S. et al., *Synthesis and characterization of crystalline Nano silica from rice husk (agricultural waste) and its magnetic composites.* 2022.

(44) Saravanan, S.; Dubey, R. Synthesis of SiO2 nanoparticles by sol-gel method and their optical and structural properties. *Rom. J. Inf. Sci. Technol* **2020**, *23*, 105−112.

(45) Yeasmin, M. N.; et al. Structural, Optical, and Morphological Characterization of Silica Nanoparticles Prepared by Sol-Gel Process. *J. Turkish Chem. Soc. Sect. A: Chem.* **2022**, *9*, 1323−1334.

(46) Tian, Y.; et al. Facile, one-pot synthesis, and antibacterial activity of mesoporous silica nanoparticles decorated with well-dispersed silver nanoparticles. *ACS Appl. Mater. Interfaces* **2014**, *6*, 12038−12045.

(47) Jeon, H.-J.; Yi, S.-C.; Oh, S.-G. Preparation and antibacterial effects of Ag−SiO2 thin films by sol−gel method. *Biomaterials* **2003**, *24*, 4921−4928.

(48) Lotfiman, S.; Ghorbanpour, M. Antimicrobial activity of ZnO/silica gel nanocomposites prepared by a simple and fast solid-state method. *Surf. Coat. Technol.* **2017**, *310*, 129−133.

(49) Babu, L. K.; et al. Hydrothermal synthesis of flower-like ZnO-SiO2 nanocomposites for solar light−induced photocatalysis and antibacterial applications. *Mater. Res. Express* **2019**, *6*, No. 0850i4.

(50) Zulfiqar, H.; et al. Synthesis of silver nanoparticles using Fagonia cretica and their antimicrobial activities. *Nanoscale Advances* **2019**, *1*, 1707−1713.

(51) Bertola, A. Rodent models of fatty liver diseases. *Liver Research* **2018**, *2*, 3−13.

(52) Priya, K. K.; et al. Ecological risk assessment of silicon dioxide nanoparticles in a freshwater fish Labeo rohita: Hematology, ionoregulation and gill Na+/K+ ATPase activity. *Ecotoxicol. Environ. Saf.* **2015**, *120*, 295−302.

(53) Andrew, G. S.; et al. Studies on changes in some haematological and plasma biochemical parameters in wistar rats fed on diets containing calcium carbide ripened mango fruits. *Int J Food Sci Nutr Eng* **2018**, *8*, 27−36.

(54) Afzal, G.; Ahmad, H. I.; Jamal, A.; Mustafa, G.; Kiran, S.; Hussain, R.; Anjum, S.; Rafay, M.; Ghaffar, A.; Saeed, S. Bisphenol A mediated histopathological, hemato-biochemical and oxidative stress in rabbits (Oryctolagus cuniculus). *Toxin Reviews* **2022**, *41*, 1067−1076.

(55) Almansour, M.; Alarifi, S.; Jarrar, B. In vivo investigation on the chronic hepatotoxicity induced by intraperitoneal administration of 10-nm silicon dioxide nanoparticles. *Int. J. Nanomed.* **2018**, *Volume 13*, 2685.

(56) Cook, J. D.; Baynes, R. D.; Skikne, B. S. Iron deficiency and the measurement of iron status. *Nutrition Research Reviews* **1992**, *5*, 198−202.

(57) Karnam, S.; Ghosh, R. C.; Mondal, S.; Mondal, M.; et al. Evaluation of subacute bisphenol−A toxicity on male reproductive system. *Vet. World* **2015**, *8*, 738.

(58) Hussain, R.; et al. Exposure to Sub-Acute Concentrations of Glyphosate Induce Clinico-Hematological, Serum Biochemical and Genotoxic Damage in Adult Cockerels. *Pak. Vet. J.* **2019**, *39*, 181.

(59) Das, S. K.; et al. Nano-silica fabricated with silver nanoparticles: antifouling adsorbent for efficient dye removal, effective water disinfection and biofouling control. *Nanoscale* **2013**, *5*, 5549−5560.

(60) Ghaffar, A.; Hussain, R.; Abbas, G.; Ahmad, M. N.; Abbas, A.; Rahim, Y.; Younus, M.; Shahid, M.; Mohiuddin, M. Cumulative Effects of Sodium Arsenate and Diammonium Phosphate on Growth Performance, Hemato-Biochemistry and Protoplasm in Commercial Layer. *Pak. Vet. J.* **2018**, *37*, 206.

(61) Sun, M.; et al. Metabolomic characteristics of hepatotoxicity in rats induced by silica nanoparticles. *Ecotoxicol. Environ. Saf.* **2021**, *208*, No. 111496.

(62) Fan, X.; et al. Effects of oral administration of polystyrene nanoplastics on plasma glucose metabolism in mice. *Chemosphere* **2022**, *288*, No. 132607.

(63) Kim, I.-Y.; Joachim, E.; Choi, H.; Kim, K. Toxicity of silica nanoparticles depends on size, dose, and cell type. *Nanomed.: Nanotechnol., Biol. Med.* **2015**, *11*, 1407−1416.

(64) Azouz, R. A.; Korany, R. M. Toxic impacts of amorphous silica nanoparticles on liver and kidney of male adult rats: an in vivo study. *Biol. Trace Elem. Res.* **2021**, *199*, 2653−2662.

(65) Çömelekoğlu, Ü.; et al. Effects of different sizes silica nanoparticle on the liver, kidney and brain in rats: Biochemical and histopathological evaluation. *J. Res. Pharm.* **2019**, *23*, 344−353.

(66) Liu, T.; et al. Smaller silica nanorattles reabsorbed by intestinal aggravate multiple organs damage. *J. Nanosci. Nanotechnol.* **2013**, *13*, 6506−6516.

(67) Nemmar, A.; et al. Oxidative stress, inflammation, and DNA damage in multiple organs of mice acutely exposed to amorphous silica nanoparticles. *Int. J. Nanomed.* **2016**, *11*, 919.

(68) Hassankhani, R.; et al. In vivo toxicity of orally administrated silicon dioxide nanoparticles in healthy adult mice. *Environ. Sci. Pollut. Res.* **2015**, *22*, 1127−1132.

(69) Yu, Y.; Duan, J.; Li, Y.; Li, Y.; Jing, L.; Yang, M.; Wang, J.; Sun, Z. Silica nanoparticles induce liver fibrosis via TGF-β1/Smad3 pathway in ICR mice. *Int. J. Nanomed.* **2017**, *Volume 12*, 6045.

(70) Waegeneers, N.; et al. Short-term biodistribution and clearance of intravenously administered silica nanoparticles. *Toxicology reports* **2018**, *5*, 632−638.

(71) Iqbal, M. Z.; Ma, X.; Chen, T.; Zhang, L.'.; Ren, W.; Xiang, L.; Wu, A. Silica-coated super-paramagnetic iron oxide nanoparticles (SPIONPs): a new type contrast agent of T 1 magnetic resonance imaging (MRI). *J. Mater. Chem. B* **2015**, *3*, 5172−5181.

(72) Pourmohammadi, K.; Abedi, E. Enzymatic modifications of gluten protein: Oxidative enzymes. *Food Chem.* **2021**, *356*, No. 129679.

(73) Iqbal, M.; et al. Glutathione metabolizing enzymes and oxidative stress in ferric nitrilotriacetate mediated hepatic injury. *Redox Report* **1996**, *2*, 385−391.

(74) Santana, M. S.; et al. A meta-analytic review of fish antioxidant defense and biotransformation systems following pesticide exposure. *Chemosphere* **2022**, *291*, No. 132730.

(75) Parveen, A.; Siddiqui, Z. A. Impact of silicon dioxide nanoparticles on growth, photosynthetic pigments, proline, activities of defense enzymes and some bacterial and fungal pathogens of tomato. *Vegetos* **2022**, 83−93.

(76) Lakmichi, H.; Bakhtaoui, F. Z.; Gadhi, C. A.; Ezoubeiri, A.; el Jahiri, Y.; el Mansouri, A.; Zrara, I.; Loutfi, K. Toxicity profile of the aqueous ethanol root extract of Corrigiola telephiifolia pourr. (Caryophyllaceae) in rodents. *J. Evidence-Based Complementary Altern. Med.* **2011**, *2011*, 1.

(77) Ghaffar, A.; Hussain, R.; Abbas, G.; Khan, R.; Akram, K.; Latif, H.; Ali, S.; Baig, S.; du, X.; Khan, A. Assessment of genotoxic and pathologic potentials of fipronil insecticide in Labeo rohita (Hamilton, 1822). *Toxin Rev.* **2021**, *40*, 1289−1300.